

GRCF: Two-Stage Group-wise Ranking and Calibration Framework for Multimodal Sentiment Analysis

Manning Gao

South China Normal University
Guangzhou 510631, China
20232005149@m.scnu.edu.cn

Leheng Zhang

South China Normal University
Guangzhou 510631, China
lehengzhang@m.scnu.edu.cn

Shiqin Han

South China Normal University
Guangzhou 510631, China
20222121019@m.scnu.edu.cn

Haifeng Hu

Sun Yat-sen University
Guangzhou 510275, China
huhaif@mail.sysu.edu.cn

Yuncheng Jiang

South China Normal University
Guangzhou 510631, China
ycjiang@scnu.edu.cn

Sijie Mai

South China Normal University
Guangzhou 510631, China
sijiemai@m.scnu.edu.cn

Abstract

Most Multimodal Sentiment Analysis research has focused on point-wise regression. While straightforward, this approach is sensitive to label noise and neglects whether one sample is more positive than another, resulting in unstable predictions and poor correlation alignment. Pairwise ordinal learning frameworks emerged to address this gap, capturing relative order by learning from comparisons. Yet, they introduce two new trade-offs: First, they assign uniform importance to all comparisons, failing to adaptively focus on hard-to-rank samples. Second, they employ static ranking margins, which fail to reflect the varying semantic distances between sentiment groups. To address this, we propose a Two-Stage Group-wise Ranking and Calibration Framework (GRCF) that adapts the philosophy of Group Relative Policy Optimization (GRPO). Our framework resolves these trade-offs by simultaneously preserving relative ordinal structure, ensuring absolute score calibration, and adaptively focusing on difficult samples. Specifically, Stage 1 introduces a GRPO-inspired Advantage-Weighted Dynamic Margin Ranking Loss to build a fine-grained ordinal structure. Stage 2 then employs an MAE-driven objective to align prediction magnitudes. To validate its generalizability, we extend GRCF to classification tasks, including multimodal humor detection and sarcasm detection. GRCF achieves state-of-the-art performance on core regression benchmarks, while also showing strong generalizability in

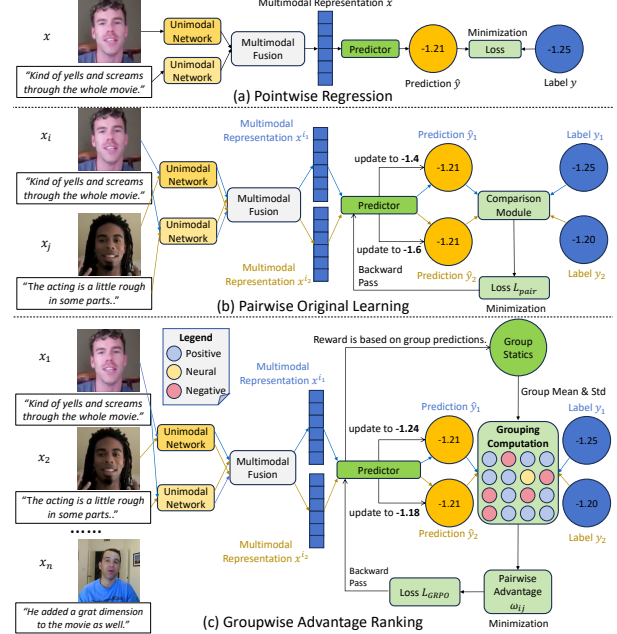


Figure 1. Comparison of optimization strategies in MSA. classification tasks.

1. Introduction

Understanding human affect through multimodal signals (language, vision, and acoustics) has been a central pursuit

in affective computing and human-centered AI. Unlike categorical perception, human emotion unfolds along a continuous, ordinal spectrum of intensity [34, 46]. Yet, despite the progress achieved by multimodal transformers [4, 37, 38] and large pre-trained encoders such as DeBERTa [12], current Multimodal Sentiment Analysis (MSA) [48] frameworks still struggle to capture this ordinal hierarchy, predicting inconsistent or poorly calibrated sentiment values.

As shown in Fig. 1, traditional MSA methods [6, 8, 14, 18] perform regression tasks directly by computing the regression loss between continuous sentiment labels and the predicted sentiment scores which treat each instance independently. Such objectives neglect relational ordering, resulting in unstable predictions, especially in circumstances near neutral. Furthermore, assigning absolute values to affective concepts is neither noise-resistant nor suitable due to their subjective and ambiguous features. Ordinal representations are more suitable for modeling affective states [46], as ranking-based approaches better accommodate the subjective and ambiguous characteristics of sentiment compared to cardinal scales. This aligns with how humans also perceive and interpret sentiment in an ordinal way. Sentiment intensity is inherently comparative: terms like “desperate” are naturally understood as more negative than “sad”, yet their exact magnitudes remain ambiguous.

To address this, recent works have explored ordinal learning, where models are encouraged to preserve monotonic sentiment relations via pair-wise constraints. Trustworthy Multimodal Sentiment Ordinal Network (TMSN) [45] and Multimodal Ordinal Affective Computing (MOAC) [25] are new endeavors. They advance MSA by incorporating ordinal reasoning from different perspectives, namely, trustworthy calibration versus direct comparison-based reasoning capacity. TMSN enhances reliability through uncertainty-guided ordinal regression, while MOAC introduces explicit comparison-based learning to model relative affective intensity. However, they rely on static ordinal constraints, treating all pair-wise relationships equally. This approach overlooks the varying semantic distances between sentiment groups, a crucial oversight given that the relationship between sentiments is inherently correlated with this distance [29]. For example, the gap between “slightly positive” (+0.5) and “strongly positive” (+3) is treated indistinctly from the gap between “neutral” (0) and “slightly positive” (+0.5). This critical distance information remains underexploited in current approaches.

Drawing inspiration from how humans perceive affective notions, we propose the Group-wise Ranking and Calibration Framework (GRCF), which simulates human focusing on similar emotional characteristics and better deals with the distance of scores between samples. It is realized by a Group-Aware Ranking Loss and later calibration.

In Stage 1, GRCF introduces an Advantage-Weighted

Dynamic Margin Ranking Loss, which adapts the core philosophy of policy gradient methods from reinforcement learning (RL) [26]. Specifically, we are inspired by Group Relative Policy Optimization (GRPO) [33]. While GRPO is often associated with sparse reward limitations, it is particularly suitable for regression because the fine-grained labels used for sentiment provide a naturally dense reward space. This dense signal, which offers nuanced preference information rather than a single sparse reward, directly mitigates the sparsity problem. For instance, MOAC asks, “Is sample i greater than sample j ?” whereas GRCF asks, “How hard is it to tell if i is greater than j and how semantically significant is the difference between i and j ?” By transforming the advantage estimate into an adaptive weight, GRCF addresses the former question by learning to prioritize only the “difficult” pairs, effectively focusing optimization on the most ambiguous samples while ignoring “easy” pairs where the ranking is already correct. As for the dynamic margin, it addresses the latter question. Overlapping ordinal groups are deliberately constructed to model the semantic ambiguity as well as homogeneity near decision boundaries, and consequently, the margin is adaptively computed based on the group memberships of the sample pairs.

In Stage 2, a Differential Calibration loss refines the manifold by aligning absolute prediction magnitudes with annotated sentiment scales without disturbing the established ordinal structure.

Experiments on CMU-MOSI [48], CMU-MOSEI [51], and CH-SIMS v2 [21] demonstrate that GRCF achieves state-of-the-art (SOTA) results. Beyond regression tasks, GRCF also extends to classification tasks such as sarcasm (MUSARD) [3] and humor detection (UR-FUNNY v2) [10], showcasing its broad generalizability.

Our main contributions are summarized as follows:

- We propose a novel idea of group-wise computing in ordinal learning. In this way, we enable the model to fully exploit inter-sample relationships.
- We devise the advantage-weighting mechanism inspired by GRPO, which controls the model to focus more on confusable samples.
- We adopt a dynamic margin realized through overlapping intervals, capturing both the semantic ambiguity and homogeneity near decision boundaries, and ensuring the margin scales proportionally with the true semantic gap.
- We adapt GRPO from its RL origins to a supervised regression framework for MSA.

2. Related Work

2.1. Point-wise MSA methods

Numerous point-wise MSA methods aim to infer human affective states by integrating textual, acoustic, and visual signals. Early fusion-based methods [14, 19, 28, 35, 52]

such as Tensor Fusion Network (TFN) [49] and Memory Fusion Network (MFN) [50] explored tensor interactions and memory mechanisms to model temporal dependencies. Transformer-based models [17, 30] like Memory Fusion Network (MuLT) [37] later introduced cross-modal attention to enable fine-grained contextual alignment. With the rise of pretrained language models, recent approaches leverage pre-trained text encoders such as BERT [5] and DeBERTa [12], coupled with lightweight acoustic and visual branches. Many other models are also devised based on pretrained language model, *e.g.*, Decoupled Multimodal Distillation (DMD) [18], Embracing Aleatoric Uncertainty (EAU)[8] and Modality-Specific Enhanced Dynamic Emotion Experts (EMOE) [6].

Despite progress, existing point-wise models fail to capture the ordinal nature of human sentiment analysis. In contrast to those point-wise models dealing with samples separately, our GRCF adopts ordinal learning to simulate the ordinal nature of human.

2.2. Ordinal and Pair-wise Ranking Learning

Sentiment prediction can be naturally formulated as an ordinal regression problem, where preserving sample order provides stronger supervision than discrete classification. Early pair-wise ranking models such as RankNet [2] and LambdaRank [31] learn monotonic score differences to maintain relative ordering. Xie *et al.* [45] devised TMSON, proposing a novel multimodal fusion framework that combines modality-specific uncertainty modeling with ordinal regression to achieve more reliable sentiment analysis in the ordinal sentiment space. Recently, Mai *et al.* [25] introduced MOAC, which formulates MSA as an ordinal learning problem by performing label-level and feature-level comparisons. Their approach demonstrates that explicitly modeling ordinal relations improves the interpretability and stability of multimodal sentiment models.

However, these pair-wise methods treat every pair equally, which contradicts human cognition. Humans tend to focus more on emotions that are harder to distinguish, and GRCF advances this direction by introducing a group-aware mechanism that adaptively adjusts pair-wise constraints based on inter-group semantic distance.

2.3. Advantage-Weighted Optimization

RL provides a flexible framework for preference-driven optimization. Algorithms such as Proximal Policy Optimization (PPO) [32] and Asynchronous Advantage Actor-Critic (A3C) [27] employ gradient weighting through advantage estimation, focusing learning on difficult samples. Recently, Shao *et al.* [33] proposed Group Relative Policy Optimization (GRPO), a variant of PPO that eliminates the need for a critic model by estimating the baseline from group scores, reducing memory consumption while achiev-

ing strong performance on mathematical reasoning tasks.

Despite satisfactory performance, GRPO suffers from sparse reward problems in discrete tasks. However, GRPO is well-suited for regression tasks like Multimodal Sentiment Analysis (MSA) [48], where continuous reward signals naturally alleviate this issue. Motivated by GRPO’s group-based advantage estimation and its applicability to regression settings, we design a deterministic variant for supervised regression. GRCF reweights pair-wise losses by normalized advantage values, offering stable and interpretable optimization without stochastic policy rollout.

3. Methodology

We propose a two-stage framework adaptable to both regression and classification: Stage 1 performs Structural Foundation to organize representations, and Stage 2 conducts Fine-Tuning. The overall pipeline is shown in Fig. 2.

3.1. Multimodal Encoder Architecture

Unimodal Encoders. Each utterance’s text T is processed by a DeBERTa-v3-base [13] encoder to produce a global textual representation \mathbf{z}_t (using the [CLS] token output). For the non-textual modalities (audio A , video V), \mathbf{z}_a and \mathbf{z}_v are produced via attention pooling:

$$\mathbf{z}_a = \sum_{i=1}^{L_a} \alpha_i^{(a)} \mathbf{A}_i \quad (1)$$

$$\alpha_i^{(a)} = \frac{\exp(\mathbf{w}_a^\top \mathbf{A}_i)}{\sum_{j=1}^{L_a} \exp(\mathbf{w}_a^\top \mathbf{A}_j)} \quad (2)$$

and analogously for \mathbf{z}_v .

Multimodal Fusion. The goal is to produce an intermediate representation, $\mathbf{z}_{\text{intermediate}}$, which is then fed into a shared unified encoder. For continuous sentiment, a holistic understanding of the context and intensity from all modalities is paramount. Regression tasks, which aim to produce a single, continuous-like score, inherently require the integration of all modalities into one unified judgment, rather than modeling discrete conflicts between them. Consequently, for this type of holistic integration task, a simple and efficient “Concatenate-then-MLP” architecture is highly effective. First, the unimodal representations are concatenated:

$$\mathbf{h}_{\text{concat}} = [\mathbf{z}_t; \mathbf{z}_a; \mathbf{z}_v] \quad (3)$$

This combined vector is then passed through a dedicated fusion MLP to create the intermediate representation:

$$\mathbf{z}_{\text{intermediate}} = \text{MLP}_{\text{fuse}}(\mathbf{h}_{\text{concat}}) \quad (4)$$

$\mathbf{z}_{\text{intermediate}}$ captures the salient multimodal information. It is then passed through a Unified Encoder (a simple MLP

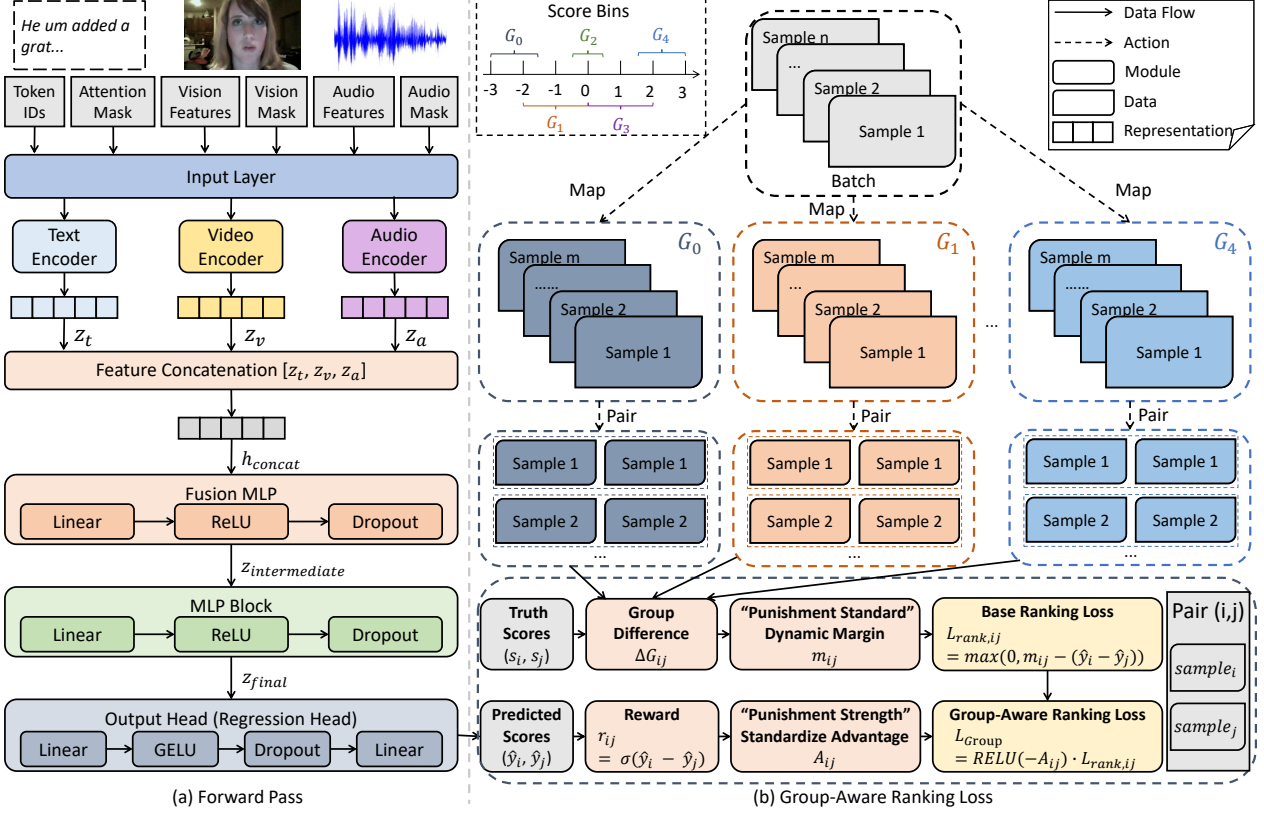


Figure 2. The forward pass model and core loss calculation which decouples the ranking “standard” from the “strength”. (a) The model processes inputs through multimodal encoders to output a predicted score. (b) For the “Punishment Standard”, ground-truth scores are mapped to overlapping groups to define the dynamic margin. For the “Punishment Strength”, predicted scores are compared against batch statistics to calculate the advantage.

block) to create the definitive representation \mathbf{z}_{final} , which is then fed into the regression head. To predict a continuous score \hat{y} , the head (a two-layer MLP) constrains the output using a scaling factor α (e.g., 3.5) and a hyperbolic tangent function to match the annotation range (e.g., [-3, 3]):

$$\hat{y} = \alpha \times \tanh(f_{reg}(\mathbf{z}_{final})) \quad (5)$$

3.2. Stage 1: Structural Foundation

The goal of Stage 1 is to address the core problem that traditional regression neglects relational ordering. Prior ordinal frameworks like MOAC [25] attempt to solve this with a complex, multi-component approach, designing separate, explicit losses for label-level ranking (L_{lo}), feature-level difference (L_{fd}), and neutral-point calibration (L_{neus}).

Instead of designing multiple, complex feature-level losses, our GRCF framework applies a single, unified loss (L_{group}) at the final output layer. Our hypothesis is that by using GRPO-inspired [33] advantage-weighting to implicitly focus on all hard-to-rank pairs (the “Punishment Strength”), the model is automatically forced to learn a robust and well-separated feature manifold. This is guided by our dynamic margin (the “Punishment Standard”), which

directly solves the “static constraint” problem of MOAC’s L_{lo} . To achieve this, the stage 1 loss function combines three key components: a core Group-Aware Ranking Loss (L_{group}) as the main engine, a Distribution Regularization Loss (L_{reg}) to anchor the entire predicted distribution and prevent “absolute drift”, and a Boundary Loss (L_{bound}) to enforce the hard annotation range on individual samples.

Group-Aware Ranking (L_{group}) This is the core loss for modeling ordinality. Its design is a multi-step process:

(1) Defining Overlapping Ordinal Groups ($g(\cdot)$): To enforce the “semantically proportional” structure mentioned above, we must first quantify semantic distance. Prior methods [20, 25, 39] treating all pairs with a static margin fail to do this. Our solution is to first realistically model the fuzzy and continuous nature of human sentiment by mapping a continuous score s_i to a set of ordinal groups, $g(s_i)$. We define $K = 5$ groups using overlapping intervals, which is a deliberate choice. This design allows a single sample to belong to multiple groups, which serves two key purposes: it captures the inherent ambiguity of a single score on a boundary (for instance, a score of $s_i = 0.2$

is assigned to both G_2 and G_3), while also ensuring that numerically-close boundary samples (e.g., -1.8 and -1.6) share a group membership, correctly identifying them as semantically similar. Specifically, the groups are defined as: G_0 [-3.0, -1.5], G_1 [-2.0, 0.0], G_2 [-0.5, 0.5], G_3 [0.0, 2.0], and G_4 [1.5, 3.0].

(2) Calculating the Dynamic Margin: For a pair-wise samples (i, j) with scores $s_i > s_j$, the group difference ΔG_{ij} is defined as the maximum semantic distance between their groups:

$$\Delta G_{ij} = \max_{G_a \in G(s_i), G_b \in G(s_j)} |G_a - G_b| \quad (6)$$

Consequently, a comparison between an ambiguous sample (e.g., $s_i = 0.2$ in G_2, G_3) and a stable sample (e.g., $s_j = 2.5$ in G_4) is robustly constrained by the largest possible semantic gap (i.e., $|4 - 2| = 2$). If two samples share any group (e.g., $s_i = -1.8$ and $s_j = -1.6$, which are both in G_0 and G_1), their ΔG_{ij} becomes 0.

The dynamic margin m_{ij} is then defined based on this group difference ΔG_{ij} :

$$m_{ij} = \begin{cases} m_{\text{intra}}, & \Delta G_{ij} = 0, \\ m_{\text{base}} + \Delta G_{ij} m_{\text{step}}, & \text{otherwise.} \end{cases} \quad (7)$$

This dynamic margin mechanism is the solution to the “static constraint” problem. Instead of treating all pairs uniformly, our margin now scales proportionally with the true semantic gap defined by the groups. This teaches the model that inter-group pairs with larger semantic gaps must have a larger predicted score difference than intra-group pairs with small gaps. The base ranking loss for the pair (i, j) is then:

$$L_{\text{rank},ij} = \max(0, m_{ij} - (\hat{y}_i - \hat{y}_j)) \quad (8)$$

(3) Applying GRPO Advantage-Weighting: Having established a standard for separation (m_{ij}), we now introduce an adaptive strength for optimization (w_{ij}) by adopting the GRPO advantage-weighting principle, a method particularly well-suited for regression tasks. Unlike in classification or standard RL where GRPO often relies on sparse 0/1 reward signals (leading to the “sparse reward” problem), our continuous sentiment labels provide a naturally dense reward space. This allows GRPO to avoid this problem and effectively learn from fine-grained differences. Furthermore, we address the limitation of prior work [25, 39, 45] that treats all comparisons with uniform importance. Instead of asking “Is $i > j$?” for all pairs (like MOAC), we adapt the GRPO philosophy to ask: “How hard is it to tell if $i > j$?” This inherent compatibility makes GRPO particularly suitable for MSA [48]. We calculate a standardized advantage A_{ij} based on the reward $r_{ij} = \sigma(\hat{y}_i - \hat{y}_j)$.

Instead of using the raw, bi-directional advantage from standard RL (which would reward “easy” pairs and penalize “hard” pairs), we transform it into a one-sided penalty weight. This adaptation is crucial: a fully bi-directional objective wastes optimization on “easy” pairs (where $A_{ij} > 0$), creating significant gradient noise that can destabilize training and mask the signal from truly difficult samples. Our one-sided penalty, in contrast, acts as an adaptive filter.

The final loss up-weights pairs with negative advantages (i.e., misordered or ambiguous samples) using the weight $w_{ij} = \text{ReLU}(-A_{ij})$:

$$L_{\text{group}} = \frac{1}{N_p} \sum_{s_i > s_j} w_{ij} \cdot L_{\text{rank},ij} \quad (9)$$

This fuzzy boundary and advantage-weighting mechanism allows our model to learn a smoother and more semantically coherent ordinal manifold.

Distribution Regularization (L_{reg}) To ensure the learned relative rankings do not “drift” in absolute terms, we regularize the predicted batch distribution (\hat{y}) to match the ground-truth batch distribution (s). This loss penalizes deviations in mean (M) and standard deviation (D) beyond a margin γ :

$$L_{\text{reg}} = [(M_p - M_r)^2 - \gamma]_+ + [(D_p - D_r)^2 - \gamma]_+ \quad (10)$$

Boundary Loss (L_{bound}) Finally, to ensure predictions remain within the valid annotation range $[-S, S]$, we add a boundary loss:

$$L_{\text{bound}} = \frac{1}{N} \sum_{i=1}^N \max(0, |\hat{y}_i| - S) \quad (11)$$

The total loss for Stage 1 is a weighted sum:

$$L_{S1} = \lambda_1 L_{\text{group}} + \lambda_2 L_{\text{reg}} + \lambda_3 L_{\text{bound}} \quad (12)$$

3.3. Stage 2: Fine-Tuning

While Stage 1 establishes a robustly structured latent space, it can suffer from a “score offset” problem. This is because Stage 1 is essentially pure ordinal learning: it focuses on relative ordering (L_{group}) and only provides a soft constraint for distributional alignment (L_{reg}), lacking a harder, point-wise calibration constraint, such as MAE, which provides a direct error gradient for every sample. Although the model uses a scaled tanh function as a hard output limit, it may still struggle to precisely anchor the absolute score distribution (e.g., the 0 point) without this direct calibration, thus causing it to drift. This dynamic is observable in the Stage 1 training curves (Fig. 3 (c)): the Boundary Loss (L_{bound})

only activates significantly in later training stages. This suggests that as the primary ranking and regularization losses converge and their gradients diminish, the uncalibrated distribution drifts until predictions begin to hit the boundaries. It is at this point that L_{bound} provides its corrective gradient.

Therefore, Stage 2’s primary role is to correct this score offset. It fine-tunes the model to optimize the MAE metric, thus calibrating the learned ordinal manifold to the absolute ground-truth scores. To prevent catastrophic forgetting of the learned structure, we employ differential learning rates, applying a higher rate to the fusion/output layers and a lower rate to the foundational encoders. To preserve the learned structure, L_{mae} is integrated with the L_{group} and L_{bound} losses from Stage 1, which now maintain the ranking ability and act as regularizer:

$$L_{S2} = \beta_1 L_{\text{mae}} + \beta_2 L_{\text{group}} + \beta_3 L_{\text{bound}} \quad (13)$$

The weight for MAE (β_1) is set significantly higher, providing a strong gradient for calibration while the other terms preserve the ordinal structure.

3.4. Extending to Classification Tasks

GRCF is suitable for regression as it applies the philosophy of GRPO to a naturally dense reward space: the continuous, fine-grained differences between sentiment scores, avoiding the sparse reward problem in typical RL applications. However, adapting GRCF to binary classification presents two challenges. First, the task reverts to a sparse, discrete reward signal (i.e., a Non-sarcastic/Sarcastic label). Second, this discrete nature invalidates the dynamic margin mechanism, as it relies on multiple fine-grained, overlapping ordinal groups (e.g., G_0 to G_4) to calculate semantic distance in regression. In binary classification, only two discrete groups exist, rendering the concept of fine-grained, overlapping inter-group intervals meaningless.

Therefore, a principled adaptation was required. We decomposed the group-wise philosophy into a Separation Loss to push inter-class clusters apart and a Compactness Loss to pull intra-class samples together. The detailed methodology is provided in the Appendix.

4. Experiments

4.1. Implementation Details

We use DeBERTa-v3-base as the text backbone; acoustic and visual features are aggregated via attention pooling and projected to a shared latent space before fusion. Training uses the AdamW optimizer with mixed precision, cosine learning-rate decay, gradient clipping, and distributed data parallelism. We conduct a two-part hyperparameter search using Optuna [1]. Stage 1 optimizes parameters to maximize pairwise accuracy, while Stage 2 is guided by minimizing MAE. Training loss curves are presented in Figure 3.

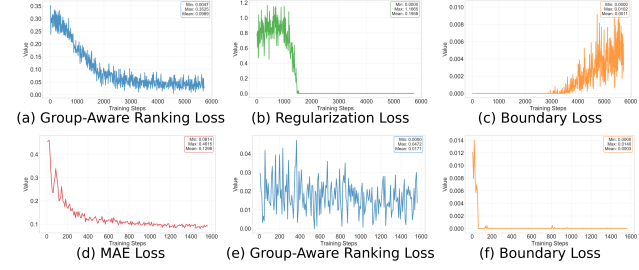


Figure 3. Training loss curves on CMU-MOSI dataset. (Top) Stage 1 loss. (Bottom) Stage 2 loss.

In Stage 1 training, the Group-Aware Ranking Loss decreases steadily, the Regularization Loss is active early in training, and the Boundary Loss activates later to penalize out-of-range predictions. In Stage 2 training, the primary MAE loss for calibration trends downward, the Group-Aware Ranking Loss remains stable, preserving the learned ranking, and the Boundary Loss is minimal, indicating few out-of-range predictions.

4.2. Main Results on MOSI/MOSEI/SIMS v2

Table 1 presents the performance of GRCF on the CMU-MOSI [48] and CMU-MOSEI [51] datasets. On the CMU-MOSI dataset, GRCF achieves SOTA results on all evaluation metrics except F1. On the CMU-MOSEI dataset, GRCF, in contrast, outperforms existing methods across all metrics, reaching SOTA levels consistently. Table 2 shows the results on the CH-SIMS v2 [21] dataset, where GRCF achieves SOTA performance on Acc3, Acc2 and F1, and tied for the best on Acc5. The superior performance is likely due to GRCF’s ordinal ranking design, which thrives on the rich, fine-grained, real-valued distinctions in the sentiment labels. These results validate the effectiveness of GRCF and its generalization across datasets.

4.3. Results on Sarcasm and Humor Detection

To evaluate the versatility of our framework, we adapt it for the binary classification tasks of Multimodal Sarcasm Detection on MUSTARD [3], and Multimodal Humor Detection on UR-FUNNY v2 [10]. It achieves an Acc2 of 75.00% on MUSTARD and 73.64% on UR-FUNNY v2, demonstrating that GRCF generalizes effectively, creating robust decision boundaries for complex classification tasks, not just for regression. Results are presented in Figure 4.

4.4. Ablation Experiment

To validate the necessity of our stage 1 components and two-stage framework, we conduct a comprehensive ablation study (results in Table 3) whose findings, supported by t-SNE visualizations in Figure 5, confirm our hypotheses.

Stage 1 Components. GRPO weighting and the dynamic margin are dependent on the complexity of the dataset’s

Table 1. The comparison with baselines on CMU-MOSI and CMU-MOSEI. Acc2 and F1 scores are calculated exclusively on positive and negative samples, with zero-valued instances excluded from the evaluation. The results labeled with \dagger are obtained from original papers, and other results are obtained from our experiments. The best results are in bold and the second best results are underlined.

Baseline Models	CMU-MOSI					CMU-MOSEI				
	Acc7 \uparrow	Acc2 \uparrow	F1 \uparrow	MAE \downarrow	Corr \uparrow	Acc7 \uparrow	Acc2 \uparrow	F1 \uparrow	MAE \downarrow	Corr \uparrow
MFM [36]	33.3	80.0	80.1	0.948	0.664	50.8	83.4	83.4	0.580	0.722
Self-MM [47]	45.8	84.9	84.8	0.731	0.785	53.0	85.2	85.2	0.540	0.763
AtCAF \dagger [15]	46.5	88.6	88.5	0.650	0.831	55.9	87.0	86.8	0.508	0.785
DLF \dagger [40]	47.1	85.1	85.0	0.731	0.781	53.9	85.4	85.3	0.536	0.764
KuDA \dagger [7]	47.1	86.4	86.5	0.705	0.795	52.9	86.5	86.6	0.529	0.776
DEVA \dagger [43]	46.3	86.3	86.3	0.730	0.787	52.3	86.1	86.2	0.541	0.769
C-MIB [23]	47.7	87.8	87.8	0.662	0.835	52.7	86.9	86.8	0.542	0.784
ITHP [44]	47.7	88.5	88.5	0.663	0.856	52.2	87.1	87.1	0.550	0.792
Multimodal Boosting [24]	49.1	88.5	88.4	0.634	0.855	54.0	86.5	86.5	0.523	0.779
CaMIB \dagger [16]	48.0	89.8	89.8	0.616	0.857	53.5	87.3	87.2	0.517	0.788
DMD [18]	44.9	84.3	84.3	0.726	0.788	52.8	84.6	84.6	0.538	0.768
EMOE [6]	45.2	84.8	84.8	0.723	0.790	52.5	85.0	85.0	0.542	0.760
TMSON \dagger [45]	47.4	87.2	87.2	0.687	0.809	55.6	86.4	86.2	0.526	0.766
MOAC \dagger [25]	48.6	89.0	89.0	0.605	0.857	54.3	87.6	87.6	0.512	0.793
GRCF	49.3	90.3	88.5	0.581	0.866	58.7	89.1	91.5	0.460	0.835

Table 2. The comparison with baselines on CH-SIMS v2.

Baseline Models	CH-SIMS v2					
	Acc5 \uparrow	Acc3 \uparrow	Acc2 \uparrow	F1 \uparrow	MAE \downarrow	Corr \uparrow
EF-LSTM [42]	53.7	73.5	80.1	80.0	0.309	0.700
LF-DNN [41]	51.8	71.2	77.8	77.9	0.322	0.668
TFN [49]	53.3	70.9	78.1	78.1	0.322	0.662
LMF [22]	51.6	70.0	77.8	77.8	0.327	0.651
MFN [50]	55.4	72.7	79.4	79.4	0.301	0.712
Graph-MFN [51]	48.9	68.6	76.6	76.6	0.334	0.644
MISA [11]	47.5	68.9	78.2	78.3	0.342	0.671
MAG-BERT [30]	49.2	70.6	77.1	77.1	0.346	0.641
Self-MM [47]	53.5	72.7	78.7	78.6	0.315	0.691
MMIM [9]	50.5	70.4	77.8	77.8	0.339	0.641
AV-MC [21]	52.1	73.2	<u>80.6</u>	<u>80.7</u>	<u>0.301</u>	0.721
KuDA [7]	53.1	74.3	80.2	80.1	0.289	0.741
GRCF	54.4	74.3	81.7	81.6	0.305	0.691

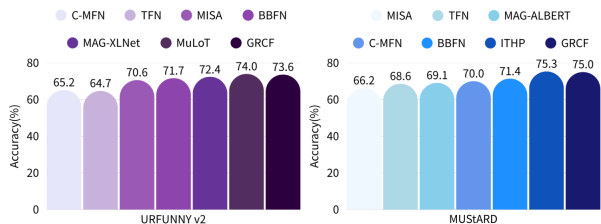


Figure 4. Main results (Acc2) on the classification tasks.

label structure and are critical for datasets with granular sentiment labels like MOSI and MOSEI (range [-3, 3]). On MOSI, removing either GRPO or the Dynamic Margin causes a substantial performance drop (e.g., -8.88% and -5.33% in Acc7, respectively). This confirms their importance in establishing a well-separated feature space for ordinal tasks. Interestingly, on CH-SIMS v2, which has a less

granular label space (range [-1, 1]), removing the key components of Stage 1 results in negligible changes or even a slight performance increase (e.g., w/o GRPO improves Corr by +1.89%). We hypothesize that for such simpler label distributions, the complex constraints imposed by GRPO and Dynamic Margin may be unnecessary, possibly introducing counter-productive optimization overhead. However, removing Stage 1 entirely still causes a distinct performance drop on SIMS v2 (e.g., -2.38% in F1), indicating that while the two key sophisticated mechanisms are not required for this simpler task, the model still benefits from the "ranking-then-calibration" framework, which provides a more stable structural foundation than direct regression alone.

Two-Stage Framework. Removing Stage 1 and relying on direct regression causes a huge performance drop (e.g., -11.55% in Acc7 on MOSI), demonstrating the necessity of the ranking-based structural foundation. Moreover, removing Stage 2 results in a catastrophic performance collapse (e.g., -43.10% in Acc3 on SIMS v2), proving that Stage 2 is indispensable for mapping ordinal space to absolute scores.

4.5. Qualitative Analysis

To provide an intuitive understanding of how our proposed components contribute to final predictions, we visualize the internal representation space via t-SNE for our full model and all four ablations in Figure 5. Instead of examining individual points, we highlight the case study samples whose ground-truth scores are smaller than < -2.0 as red "X"s.

(a) Full Model: Our full model enhances the structure established by Stage 1. The case study cluster in (a) is visibly more compact than the "ranking-only" cluster in (e). This shows that L_{mae} not only aligns the absolute scores but

Table 3. Ablation Study Results on regression tasks.

Method	CMU-MOSI			CMU-MOSEI			CH-SIMS v2		
	Acc7↑	F1↑	Corr↑	Acc7↑	F1↑	Corr↑	Acc3↑	F1↑	Corr↑
Full Model	49.3	88.5	0.866	58.7	91.5	0.835	74.3	81.6	0.691
w/o GRPO	45.0 (-8.72%)	84.2 (-4.86%)	0.835 (-3.58%)	53.9 (-8.18%)	89.5 (-2.19%)	0.736 (-11.86%)	74.4 (0.13%)	81.7 (0.12%)	0.705 (2.03%)
w/o DM	46.7 (-5.27%)	88.1 (-0.45%)	0.849 (-1.96%)	53.9 (-8.18%)	89.8 (-1.86%)	0.749 (-10.30%)	74.3 (0.00%)	81.7 (0.12%)	0.695 (0.58%)
w/o Stage 1	43.6 (-11.56%)	87.2 (-1.47%)	0.852 (-1.62%)	52.9 (-9.88%)	88.9 (-2.84%)	0.729 (-12.69%)	72.5 (-2.42%)	79.7 (-2.33%)	0.682 (-1.30%)
w/o Stage 2	37.7 (-23.53%)	88.4 (-0.11%)	0.855 (-1.27%)	42.5 (-27.60%)	86.8 (-5.14%)	0.695 (-16.77%)	42.3 (-43.07%)	31.7 (-61.15%)	0.634 (-8.25%)

also acts as a fine-tuning mechanism, further improving the intra-class compactness of the learned manifold.

(b) w/o GRPO & (c) w/o Dynamic Margin: These reveal why L_{group} is effective. Removing GRPO weighting or the dynamic margin causes the well-defined red “X” cluster to disintegrate and mix with neutral and even positive samples. This highlights two findings: 1) The GRPO weighting is critical for policing boundaries by forcing the model to resolve hard-to-rank pairs near the neutral zone. 2) The dynamic margin is essential for enforcing a semantically proportional structure, ensuring the separation between distant groups (e.g., G_0, G_2) is larger than between adjacent ones (G_0, G_1). Without this, the single static margin causes the cluster to “leak”, as seen in (c).

(d) w/o Stage 1: It represents a complete structural failure. The case study samples are chaotically scattered across the entire representation space, indiscriminately mixing with “neutral” and even “positive” samples, demonstrating that L_{mae} is incapable of learning a semantically meaningful or ordinally-aware manifold.

(e) w/o Stage 2: In contrast to the chaos of (d), applying only Stage 1 results in a dramatic structural organization. The case study samples spontaneously collapse into a distinct, well-separated cluster on the far right, proving that the Stage 1 design is responsible for creating the foundational ordinal manifold, successfully separating semantic groups.

In summary, this demonstrates that our components are not redundant but symbiotic. Stage 1 builds the ordinal structure that direct regression (d) completely misses. Stage 2 then refines this structure, leading to the highly compact and well-separated representations of the full model (a).

4.6. Analysis of Dynamic Margin Mechanism

To investigate how different grouping strategies for the dynamic margin affect performance, we conducted a comparative experiment on CMU-MOSI dataset (Table 4). We compare “Overlap, 5” strategy (detailed in the Methodology 3) against three variants:

- “Overlap, 3” and “Overlap, 7”: Use 3 and 7 overlapping bins, respectively, to test granularity.

Table 4. Comparison of different dynamic margin strategies.

Strategy	Acc7↑	Acc2↑	F1↑	MAE↓	Corr↑
Overlap, 5	49.3	90.3	88.5	0.580	0.866
Overlap, 3	46.1	88.9	87.4	0.623	0.845
Overlap, 7	46.1	88.7	87.2	0.623	0.847
Strict, 5	46.1	88.4	86.9	0.623	0.848

- “Strict, 5”: Uses 5 non-overlapping bins (e.g., [-3.0, -1.8), [-1.8, -0.6), ...) to test the importance of the overlap itself. The results in Table 4 strongly validate that our “Overlap, 5” strategy significantly outperforms all other configurations across all metrics (e.g., 49.34 Acc7). The “Strict, 5” strategy’s performance drop (46.27 Acc7) confirms that modeling semantic ambiguity via overlapping intervals is critical. Furthermore, the degraded results from “Overlap, 3” and “Overlap, 7” suggest that 5 bins provide the optimal granularity for capturing the sentiment spectrum.

4.7. Robustness to Input Noise

To evaluate GRCF’s robustness against real-world sensor artifacts, we inject additive Gaussian input noise $N(0, \sigma^2)$ with varying standard deviations (σ) into the unimodal non-textual features. The results are presented in Table 5.

Performance remains remarkably stable with minimal degradation, even at high noise levels. On CMU-MOSEI, the model is notably insensitive, showing no performance change in MAE or Corr up to $\sigma = 0.3$, suggesting a highly robust learned representation. Interestingly, we observe a slight regularization effect on CMU-MOSI, where noise at $\sigma = 0.3$ marginally improves both metrics. This suggests that the noise may help the model disregard spurious, non-generalizable artifacts. In summary, the framework’s ability to withstand and, in some cases, leverage input noise demonstrates its high robustness.

5. Conclusion and Future Work

In this work, we introduced two-stage GRCF, which adapts the group-wise philosophy for ordinal representation learning in MSA. Our core innovation is the Group-Aware

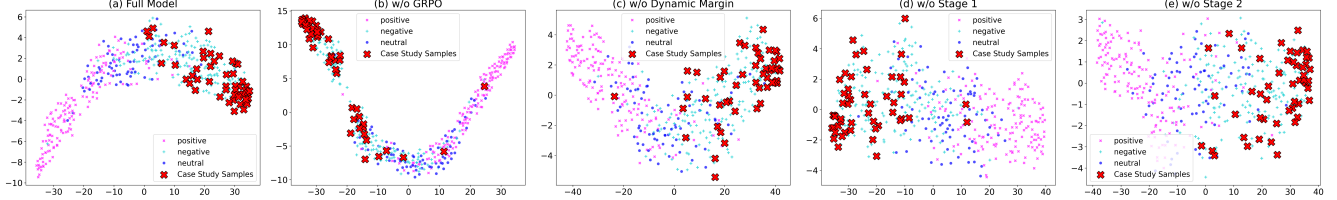


Figure 5. t-SNE visualization of ablations on CMU-MOSI. (a) Full model. Component ablations of Group-Aware Ranking Loss: (b) Ablating GRPO advantage-weighting. (c) Ablating dynamic margin. Strategy ablations: (d) Direct regression. (e) Stage 1 alone.

Table 5. Robustness to Gaussian noise on non-textual modalities.

Noise	CMU-MOSI		CMU-MOSEI		CH-SIMS v2	
	MAE	Corr	MAE	Corr	MAE	Corr
0	0.581	0.866	0.461	0.835	0.305	0.691
0.01	0.581	0.866	0.461	0.835	0.305	0.691
0.05	0.581	0.866	0.461	0.835	0.306	0.691
0.1	0.582	0.866	0.461	0.835	0.305	0.691
0.15	0.581	0.865	0.461	0.835	0.305	0.692
0.2	0.583	0.866	0.461	0.835	0.305	0.692
0.3	0.577	0.867	0.461	0.835	0.305	0.691

Ranking Loss, which builds an ordinally-consistent foundation by simultaneously adaptively focusing on hard-to-rank pairs via advantage-weighting and enforcing semantically-proportional distances via a dynamic margin. GRCF achieves strong performance on regression benchmarks and demonstrates clear generalizability to classification tasks.

A future direction is to improve the difficulty ranking principle for classification, which currently suffers from a sparse reward bottleneck. This will involve creating a pseudo-dense ordinal signal based on sample difficulty (e.g., cross-modal conflict) to unlock the full potential of our GRPO-inspired advantage weighting mechanism.

References

- [1] Takuya Akiba, Shotaro Sano, Toshihiko Yanase, Takeru Ohta, and Masanori Koyama. Optuna: A next-generation hyperparameter optimization framework. In *KDD*, 2019. [6](#)
- [2] Chris Burges, Tal Shaked, Erin Renshaw, Ari Lazier, Matt Deeds, Nicole Hamilton, and Greg Hullender. Learning to rank using gradient descent. In *Proceedings of the 22nd international conference on Machine learning*, pages 89–96, 2005. [3](#)
- [3] Santiago Castro, Devamanyu Hazarika, Verónica Pérez-Rosas, Roger Zimmermann, Rada Mihalcea, and Soujanya Poria. Towards multimodal sarcasm detection (an ‘Obviously’ perfect paper). In *Proceedings of the 57th Annual Meeting of the Association for Computational Linguistics*, pages 4619–4629, Florence, Italy, 2019. Association for Computational Linguistics. [2, 6, 5](#)
- [4] Junyan Cheng, Iordanis Fostiropoulos, Barry Boehm, and Mohammad Soleymani. Multimodal phased transformer for sentiment analysis. In *Proceedings of the 2021 Conference on Empirical Methods in Natural Language Processing and the 9th International Joint Conference on Natural Language Processing (EMNLP-IJCNLP)*, pages 2046–2056, Hong Kong, China, 2019. Association for Computational Linguistics. [2, 6, 5](#)
- [5] Jacob Devlin, Ming-Wei Chang, Kenton Lee, and Kristina Toutanova. BERT: Pre-training of deep bidirectional transformers for language understanding. In *Proceedings of the 2019 Conference of the North American Chapter of the Association for Computational Linguistics: Human Language Technologies, Volume 1 (Long and Short Papers)*, pages 4171–4186, Minneapolis, Minnesota, 2019. Association for Computational Linguistics. [3](#)
- [6] Yiyang Fang, Wenke Huang, Guancheng Wan, Kehua Su, and Mang Ye. Emoe: Modality-specific enhanced dynamic emotion experts. In *Proceedings of the Computer Vision and Pattern Recognition Conference (CVPR)*, pages 14314–14324, 2025. [2, 3, 7](#)
- [7] Xinyu Feng, Yuming Lin, Lihua He, You Li, Liang Chang, and Ya Zhou. Knowledge-guided dynamic modality attention fusion framework for multimodal sentiment analysis. In *Findings of the Association for Computational Linguistics: EMNLP 2024*, pages 14755–14766, Miami, Florida, USA, 2024. Association for Computational Linguistics. [7, 6](#)
- [8] Zixian Gao, Xun Jiang, Xing Xu, Fumin Shen, Yujie Li, and Heng Tao Shen. Embracing unimodal aleatoric uncertainty for robust multimodal fusion. In *Proceedings of the IEEE/CVF Conference on Computer Vision and Pattern Recognition (CVPR)*, pages 26876–26885, 2024. [2, 3](#)
- [9] Wei Han, Hui Chen, and Soujanya Poria. Improving multimodal fusion with hierarchical mutual information maximization for multimodal sentiment analysis. In *Proceedings of the 2021 Conference on Empirical Methods in Natural Language Processing*, pages 9180–9192, Online and Punta Cana, Dominican Republic, 2021. Association for Computational Linguistics. [7, 8](#)
- [10] Md Kamrul Hasan, Wasifur Rahman, AmirAli Bagher Zadeh, Jianyuan Zhong, Md Iftekhar Tanveer, Louis-Philippe Morency, and Mohammed (Ehsan) Hoque. UR-FUNNY: A multimodal language dataset for understanding humor. In *Proceedings of the 2019 Conference on Empirical Methods in Natural Language Processing and the 9th International Joint Conference on Natural Language Processing (EMNLP-IJCNLP)*, pages 2046–2056, Hong Kong, China, 2019. Association for Computational Linguistics. [2, 6, 5](#)
- [11] Devamanyu Hazarika, Roger Zimmermann, and Soujanya Poria. Misa: Modality-invariant and-specific representations for multimodal sentiment analysis. In *Proceedings of the Conference on Empirical Methods in Natural Language Processing*, pages 2447–2458, 2021. [2](#)

28th ACM international conference on multimedia, pages 1122–1131, 2020. 7, 8

[12] Pengcheng He, Xiaodong Liu, Jianfeng Gao, and Weizhu Chen. Deberta: Decoding-enhanced bert with disentangled attention. In *International Conference on Learning Representations*, 2021. 2, 3

[13] Pengcheng He, Jianfeng Gao, and Weizhu Chen. DeBERTav3: Improving debERTa using ELECTRA-style pre-training with gradient-disentangled embedding sharing. In *The Eleventh International Conference on Learning Representations*, 2023. 3

[14] Ming Hou, Jiajia Tang, Jianhai Zhang, Wanzeng Kong, and Qibin Zhao. Deep multimodal multilinear fusion with high-order polynomial pooling. *Advances in Neural Information Processing Systems*, 32, 2019. 2

[15] Changqin Huang, Jili Chen, Qionghao Huang, Shijin Wang, Yaxin Tu, and Xiaodi Huang. Atcaf: Attention-based causality-aware fusion network for multimodal sentiment analysis. *Information Fusion*, 114:102725, 2025. 7, 6

[16] Menghua Jiang, Yuncheng Jiang, Haifeng Hu, and Sijie Mai. Towards minimal causal representations for human multimodal language understanding. *CoRR*, abs/2509.21805, 2025. 7, 4, 5

[17] Sixia Li and Shogo Okada. Interpretable multimodal sentiment analysis based on textual modality descriptions by using large-scale language models. *arXiv preprint arXiv:2305.06162*, 2023. 3

[18] Yong Li, Yuanzhi Wang, and Zhen Cui. Decoupled multimodal distilling for emotion recognition. In *Proceedings of the IEEE/CVF conference on computer vision and pattern recognition*, pages 6631–6640, 2023. 2, 3, 7

[19] Paul Pu Liang, Zhun Liu, Yao-Hung Hubert Tsai, Qibin Zhao, Ruslan Salakhutdinov, and Louis-Philippe Morency. Learning representations from imperfect time series data via tensor rank regularization. In *Proceedings of the 57th Annual Meeting of the Association for Computational Linguistics*, pages 1569–1576, Florence, Italy, 2019. Association for Computational Linguistics. 2

[20] Weiyang Liu, Yandong Wen, Zhiding Yu, and Meng Yang. Large-margin softmax loss for convolutional neural networks. In *Proceedings of the 33rd International Conference on International Conference on Machine Learning-Volume 48*, pages 507–516, 2016. 4

[21] Yihe Liu, Ziqi Yuan, Huisheng Mao, Zhiyun Liang, Wanqiyue Yang, Yuanzhe Qiu, Tie Cheng, Xiaoteng Li, Hua Xu, and Kai Gao. Make acoustic and visual cues matter: Ch-sims v2. 0 dataset and av-mixup consistent module. In *Proceedings of the 2022 international conference on multimodal interaction*, pages 247–258, 2022. 2, 6, 7, 3, 5, 8

[22] Zhun Liu, Ying Shen, Varun Bharadhwaj Lakshminarasimhan, Paul Pu Liang, AmirAli Bagher Zadeh, and Louis-Philippe Morency. Efficient low-rank multimodal fusion with modality-specific factors. In *Proceedings of the 56th Annual Meeting of the Association for Computational Linguistics (Volume 1: Long Papers)*, pages 2247–2256, 2018. 7, 8

[23] Sijie Mai, Ying Zeng, and Haifeng Hu. Multimodal information bottleneck: Learning minimal sufficient unimodal and multimodal representations. *IEEE Transactions on Multimedia*, 25:4121–4134, 2023. 7

[24] Sijie Mai, Ya Sun, Aolin Xiong, Ying Zeng, and Haifeng Hu. Multimodal boosting: Addressing noisy modalities and identifying modality contribution. *IEEE Transactions on Multimedia*, 26:3018–3033, 2024. 7

[25] Sijie Mai, Ying Zeng, and Haifeng Hu. Learning by comparing: Boosting multimodal affective computing through ordinal learning. In *Proceedings of the ACM on Web Conference 2025*, pages 2120–2134, 2025. 2, 3, 4, 5, 7

[26] Volodymyr Mnih, Koray Kavukcuoglu, David Silver, Andrei A Rusu, Joel Veness, Marc G Bellemare, Alex Graves, Martin Riedmiller, Andreas K Fidjeland, Georg Ostrovski, et al. Human-level control through deep reinforcement learning. *nature*, 518(7540):529–533, 2015. 2

[27] Volodymyr Mnih, Adria Puigdomenech Badia, Mehdi Mirza, Alex Graves, Timothy Lillicrap, Tim Harley, David Silver, and Koray Kavukcuoglu. Asynchronous methods for deep reinforcement learning. In *International conference on machine learning*, pages 1928–1937. PMLR, 2016. 3

[28] Soujanya Poria, Erik Cambria, Rajiv Bajpai, and Amir Hussain. A review of affective computing: From unimodal analysis to multimodal fusion. *Information fusion*, 37:98–125, 2017. 2

[29] Jonathan Posner, James A Russell, and Bradley S Peterson. The circumplex model of affect: An integrative approach to affective neuroscience, cognitive development, and psychopathology. *Development and psychopathology*, 17(3):715–734, 2005. 2

[30] Wasifur Rahman, Md Kamrul Hasan, Sangwu Lee, Amir Zadeh, Chengfeng Mao, Louis-Philippe Morency, and Ehsan Hoque. Integrating multimodal information in large pre-trained transformers. In *Proceedings of the conference. Association for Computational Linguistics. Meeting*, page 2359. NIH Public Access, 2020. 3, 7, 8

[31] Bernhard Schölkopf, John Platt, and Thomas Hofmann. *Advances in neural information processing systems 19: Proceedings of the 2006 conference*. MIT press, 2007. 3

[32] John Schulman, Filip Wolski, Prafulla Dhariwal, Alec Radford, and Oleg Klimov. Proximal policy optimization algorithms. *arXiv preprint arXiv:1707.06347*, 2017. 3

[33] Zhihong Shao, Peiyi Wang, Qihao Zhu, Runxin Xu, Junxiao Song, Xiao Bi, Haowei Zhang, Mingchuan Zhang, YK Li, Yang Wu, et al. Deepseekmath: Pushing the limits of mathematical reasoning in open language models. *arXiv preprint arXiv:2402.03300*, 2024. 2, 3, 4, 1

[34] Niklas Stoehr, Ryan Cotterell, and Aaron Schein. Sentiment as an ordinal latent variable. In *Proceedings of the 17th Conference of the European Chapter of the Association for Computational Linguistics*, pages 103–115, 2023. 2

[35] Hao Sun, Hongyi Wang, Jiaqing Liu, Yen-Wei Chen, and Lanfen Lin. Cubemlp: An mlp-based model for multimodal sentiment analysis and depression estimation. In *Proceedings of the 30th ACM international conference on multimedia*, pages 3722–3729, 2022. 2

[36] Yao-Hung Hubert Tsai, Paul Pu Liang, Amir Zadeh, Louis-Philippe Morency, and Ruslan Salakhutdinov. Learning factorized multimodal representations. In *ICLR*, 2019. 7, 6

[37] Yao-Hung Hubert Tsai, Shaojie Bai, Paul Pu Liang, J Zico Kolter, Louis-Philippe Morency, and Ruslan Salakhutdinov. Multimodal transformer for unaligned multimodal language sequences. In *Proceedings of the conference. Association for computational linguistics. Meeting*, page 6558, 2019. [2](#), [3](#)

[38] Ashish Vaswani, Noam Shazeer, Niki Parmar, Jakob Uszkoreit, Llion Jones, Aidan N Gomez, Łukasz Kaiser, and Illia Polosukhin. Attention is all you need. *Advances in neural information processing systems*, 30, 2017. [2](#)

[39] Feng Wang and Huaping Liu. Understanding the behaviour of contrastive loss. In *Proceedings of the IEEE/CVF conference on computer vision and pattern recognition*, pages 2495–2504, 2021. [4](#), [5](#)

[40] Pan Wang, Qiang Zhou, Yawen Wu, Tianlong Chen, and Jingtong Hu. Dlf: Disentangled-language-focused multimodal sentiment analysis. In *Proceedings of the AAAI Conference on Artificial Intelligence*, pages 21180–21188, 2025. [7](#), [6](#)

[41] Jennifer Williams, Ramona Comanescu, Oana Radu, and Leimin Tian. Dnn multimodal fusion techniques for predicting video sentiment. In *Proceedings of grand challenge and workshop on human multimodal language (Challenge-HML)*, pages 64–72, 2018. [7](#), [8](#)

[42] Jennifer Williams, Steven Kleinegesse, Ramona Comanescu, and Oana Radu. Recognizing emotions in video using multimodal dnn feature fusion. In *Proceedings of Grand Challenge and Workshop on Human Multimodal Language (Challenge-HML)*, pages 11–19, 2018. [7](#), [8](#)

[43] Sheng Wu, Dongxiao He, Xiaobao Wang, Longbiao Wang, and Jianwu Dang. Enriching multimodal sentiment analysis through textual emotional descriptions of visual-audio content. In *Proceedings of the AAAI Conference on Artificial Intelligence*, pages 1601–1609, 2025. [7](#), [6](#)

[44] Xiongye Xiao, Gengshuo Liu, Gaurav Gupta, Defu Cao, Shixuan Li, Yaxing Li, Tianqing Fang, Mingxi Cheng, and Paul Bogdan. Neuro-inspired information-theoretic hierarchical perception for multimodal learning. In *The Twelfth International Conference on Learning Representations*, 2024. [7](#), [4](#), [5](#)

[45] Zhuyang Xie, Yan Yang, Jie Wang, Xiaorong Liu, and Xiaofan Li. Trustworthy multimodal fusion for sentiment analysis in ordinal sentiment space. *IEEE Transactions on Circuits and Systems for Video Technology*, 34(8):7657–7670, 2024. [2](#), [3](#), [5](#), [7](#)

[46] Georgios N Yannakakis, Roddy Cowie, and Carlos Busso. The ordinal nature of emotions: An emerging approach. *IEEE Transactions on Affective Computing*, 12(1):16–35, 2018. [2](#)

[47] Wenmeng Yu, Hua Xu, Ziqi Yuan, and Jiele Wu. Learning modality-specific representations with self-supervised multi-task learning for multimodal sentiment analysis. In *Proceedings of the AAAI conference on artificial intelligence*, pages 10790–10797, 2021. [7](#), [6](#)

[48] Amir Zadeh, Rowan Zellers, Eli Pincus, and Louis-Philippe Morency. Multimodal sentiment intensity analysis in videos: Facial gestures and verbal messages. *IEEE Intelligent Systems*, 31(6):82–88, 2016. [2](#), [3](#), [5](#), [6](#)

[49] Amir Zadeh, Minghai Chen, Soujanya Poria, Erik Cambria, and Louis-Philippe Morency. Tensor fusion network for multimodal sentiment analysis. In *Proceedings of the 2017 Conference on Empirical Methods in Natural Language Processing*, pages 1103–1114, 2017. [3](#), [7](#), [8](#)

[50] Amir Zadeh, Paul Pu Liang, Navonil Mazumder, Soujanya Poria, Erik Cambria, and Louis-Philippe Morency. Memory fusion network for multi-view sequential learning. In *Proceedings of the AAAI conference on artificial intelligence*, 2018. [3](#), [7](#), [8](#)

[51] AmirAli Bagher Zadeh, Paul Pu Liang, Soujanya Poria, Erik Cambria, and Louis-Philippe Morency. Multimodal language analysis in the wild: Cmu-mosei dataset and interpretable dynamic fusion graph. In *Proceedings of the 56th Annual Meeting of the Association for Computational Linguistics (Volume 1: Long Papers)*, pages 2236–2246, 2018. [2](#), [6](#), [7](#), [5](#), [8](#)

[52] Linan Zhu, Zhechao Zhu, Chenwei Zhang, Yifei Xu, and Xiangjie Kong. Multimodal sentiment analysis based on fusion methods: A survey. *Information Fusion*, 95:306–325, 2023. [2](#)

GRCF: Two-Stage Group-wise Ranking and Calibration Framework for Multimodal Sentiment Analysis

Supplementary Material

Appendix A: Methodology for Classification

A.1 Multimodal Fusion: Gated Cross-Attention

Binary classification tasks often rely on subtle inter-modal cues and must resolve potential sentiment conflicts between modalities (*e.g.*, sarcastic positive text with a negative tone). We therefore employ a more sophisticated Gated Cross-Attention (GCA) mechanism. This allows the model to dynamically adjudicate and balance the influence of text versus other modalities.

To fuse modalities, we first derive a base text representation, \mathbf{z}_{text} , by mean-pooling the text encoder’s output. A fused representation, $\mathbf{z}_{\text{fused}}$, is then generated by having the text representation attend to the processed non-textual modalities ($\mathbf{z}_{\text{non-text}}$) via a cross-attention module:

$$\mathbf{z}_{\text{fused}} = \text{CrossAttention}(\mathbf{Q} = \mathbf{z}_{\text{text}}, \mathbf{K}/\mathbf{V} = \mathbf{z}_{\text{non-text}}) \quad (14)$$

where \mathbf{Q} , \mathbf{K} and \mathbf{V} refer to Query, Key, and Value respectively. Concurrently, a dynamic gate, g , is calculated by an MLP that learns the relative importance of the pure text versus the fused representation by observing both:

$$g = \sigma(\text{MLP}(\text{Concat}(\mathbf{z}_{\text{text}}, \mathbf{z}_{\text{fused}}))) \quad (15)$$

The final multimodal representation, $\mathbf{z}_{\text{final}}$, is a weighted sum that allows the model to favor either the text-only signal or the cross-modal fused signal on a per-sample basis:

$$\mathbf{z}_{\text{final}} = (g \cdot \mathbf{z}_{\text{text}}) + ((1 - g) \cdot \mathbf{z}_{\text{fused}}) \quad (16)$$

The final prediction logits, \hat{y} , are then generated from this dynamically balanced representation $\mathbf{z}_{\text{final}}$.

A.2 Stage 1: Structural Foundation

The Stage 1 objective for classification is designed to create a well-structured latent space where positive and negative samples are clearly distinct and internally coherent. The total loss is a weighted sum of four components:

$$L_{S1} = \theta_1 L_{\text{sep}} + \theta_2 L_{\text{comp}} + \theta_3 L_{\text{bound}} + \theta_4 L_{\text{cal}} \quad (17)$$

where θ_i are hyperparameter weights. The components are defined as:

- **Separation Loss (L_{sep}):** This loss operates on heterogeneous pairs (i, j) where labels $s_i \neq s_j$. It adapts the GRPO [33] philosophy by applying a weighted margin loss. For a given pair, let $(\hat{y}_{\text{pos}}, \hat{y}_{\text{neg}})$ be the predicted

logits for the positive and negative samples, respectively. The base loss is a hinge loss:

$$L_{\text{rank}} = \max(0, m_{\text{sep}} - (\hat{y}_{\text{pos}} - \hat{y}_{\text{neg}})) \quad (18)$$

where m_{sep} is a fixed margin. This loss is then weighted by a measure of “difficulty” w , which is derived from the sigmoid-based reward:

$$w = 1.0 - \sigma(\hat{y}_{\text{pos}} - \hat{y}_{\text{neg}}) \quad (19)$$

The final loss is the expectation of the weighted hinge loss, prioritizing misordered or ambiguous pairs:

$$L_{\text{sep}} = \mathbb{E}[w \cdot L_{\text{rank}}] \quad (20)$$

- **Compactness Loss (L_{comp}):** This loss operates on homogeneous pairs (i, j) where labels $s_i = s_j$. Its goal is to minimize intra-class variance. The base loss is the squared distance:

$$L_{\text{dist}} = (\hat{y}_i - \hat{y}_j)^2 \quad (21)$$

This loss is weighted by a reward mechanism, $r_{\text{comp}} = \exp(-L_{\text{dist}})$, and its corresponding advantage A , which is normalized and clipped:

$$A = \text{clip}\left(\frac{r_{\text{comp}} - \mathbb{E}[r_{\text{comp}}]}{\text{std}(r_{\text{comp}}) + \epsilon}, -A_{\text{clip}}, A_{\text{clip}}\right) \quad (22)$$

The final loss penalizes pairs within the same class that are predicted to be too far apart by weighting the base loss by the negative advantage:

$$L_{\text{comp}} = \mathbb{E}[\max(0, L_{\text{dist}} \cdot (-A))] \quad (23)$$

- **Boundary Loss (L_{bound}):** This is a positioning loss. It enforces absolute score positioning by penalizing positive predictions $\hat{y}_{\text{pos}} < m_b$ and negative predictions $\hat{y}_{\text{neg}} > -m_b$, where m_b is a boundary margin.

$$L_{\text{bound}} = \mathbb{E}_{\hat{y}_{\text{pos}}}[\max(0, m_b - \hat{y}_{\text{pos}})] + \mathbb{E}_{\hat{y}_{\text{neg}}}[\max(0, \hat{y}_{\text{neg}} + m_b)] \quad (24)$$

- **Calibration Loss (L_{cal}):** A simple regularization term which encourages the mean of all predictions \hat{y} in a batch to be centered at zero.

$$L_{\text{cal}} = |\mathbb{E}[\hat{y}]| = \left| \frac{1}{N_{\text{batch}}} \sum_{i=1}^{N_{\text{batch}}} \hat{y}_i \right| \quad (25)$$

A.3 Stage 2: Fine-Tuning

The goal for classification is to fine-tune the decision boundary for the specific binary task. Therefore, Stage 2 employs a Binary Cross Entropy (BCE) Loss:

$$L_{S2} = -\frac{1}{N} \sum_{i=1}^N [s_i \cdot \log(\sigma(\hat{y}_i)) + (1 - s_i) \cdot \log(1 - \sigma(\hat{y}_i))] \quad (26)$$

This stage uses differential learning rates, applying a smaller rate to the pre-trained text encoder and a larger rate to the fusion and classification head parameters, to achieve robust convergence without catastrophically forgetting the structure learned in Stage 1.

Appendix B: Additional Experiments

B.1 Analysis of GRPO Advantage-Weighting

To gain a deeper understanding of how the GRPO advantage-weighting mechanism ($w_{ij} = \text{ReLU}(-A_{ij})$) focuses on “hard sample pairs”, we analyze the properties of the pairs with the top 5% highest GRPO weights from CMU-MOSI (Multimodal Sentiment Analysis, MSA) [48] and all heterogeneous pairs from MUStARD (Multimodal Sarcasm Detection, MSD) [3]. We hypothesize that the definition of a “hard sample pair” is task-dependent, changing based on the intrinsic challenge of the task.

- For MSA, a task defined by modality congruence, we hypothesize the challenge is distinguishing fine-grained emotional degrees (i.e., score proximity).
- For MSD, a task defined by modality incongruity (e.g., positive text + negative tone), we hypothesize the challenge is resolving inter-modal semantic conflict (i.e., modality conflict).

Our experimental results confirm both hypotheses.

On MSA: Difficulty is Driven by Fine-Grained Proximity

For the CMU-MOSI, we conducted a multiple regression analysis to disentangle whether the GRPO-assigned “hard sample pairs weight” was driven by score proximity or modality conflict count.

Our primary evidence comes from a multiple regression analysis detailed in Table 6. When both score proximity and conflict count were used as predictors for weight, score proximity emerged as the only statistically significant factor ($p = 0.019$). In contrast, conflict count was not significant ($p = 0.361$), indicating it provides no independent explanatory power over the variance in difficulty. The model’s R-squared is expectedly low at 0.002. This is because the analysis was performed only on the “top 5% hard sample pairs”, a highly filtered and homogeneous subset. As visualized in Figure 6(a), the dependent variable (“Weight”) has minimal

variance within this group, with most values tightly clustered between 1.8 and 2.0. The purpose of this OLS analysis was not to build a predictive model (which requires a high R-squared), but to test the statistical significance of its predictors. This conclusion is further supported by a direct Spearman correlation analysis between weight and conflict count, which shows a negligible correlation ($\rho = 0.0104$). The boxplot (Figure 6(a)) and trend plot (b) both confirm this lack of relationship, showing a nearly identical weight distribution regardless of the conflict count.

Finally, an analysis of the distribution of hard pairs (Figure 6(c)) reveals a diverse mix of sources. “No Conflict” pairs account for 14.46% of hard pairs, a substantial portion comparable to major conflict types like “Vision Disagrees” (16.19%). This demonstrates that difficulty (high weight) is not exclusively caused by conflict; a significant portion arises from pairs that are congruent but semantically close.

In a congruent task like MSA, the true challenge is not inter-modal conflict, but distinguishing fine-grained scores. The OLS regression ($p = 0.361$) and negligible Spearman correlation ($\rho = 0.0104$) strongly confirm that GRPO advantage-weighting successfully identifies these semantically close pairs as the “hard sample pairs” to prioritize.

Table 6. Statistical analysis of predictors for the GRPO-inspired advantage weights of sample pairs on CMU-MOSI. OLS regression confirms score proximity as the only significant factor.

Variable	Coefficient	Std. Err.	t-statistic	P > t
Const	1.8443	0.007	278.811	< 0.001
Score Proximity	1.743e-08	7.43e-09	2.345	0.019
Conflict Count	0.0040	0.004	0.913	0.361

N = 3125 (top 5% hard pairs)

R-squared: 0.002

Spearman’s ρ (Weight vs. Conflict Count): 0.0104

On MSD: Difficulty is Driven by Modality Conflict

For the MUStARD, the same analysis reveals the opposite trend, as sarcasm is inherently defined by incongruity between what is said (Text) and how it is said (Vision, Audio).

The results in Table 7 show a strong and positive correlation ($\rho = 0.1659$) between the GRPO weight and the modality conflict count. The mean GRPO weight increases dramatically with the level of conflict: pairs with one conflict (0.0190) are over 2.2 times harder than non-conflicting pairs (0.0085), and this penalty escalates to 5.9 times for pairs exhibiting two conflicts (0.0500). In the most extreme cases, the average weight reaches 0.4445, exceeding the non-conflicting average by over 52 times. As shown in Table 8, this trend is also evident in specific modality conflict breakdowns, as T-V incongruent pairs receive an average weight (0.0210) nearly double that of T-V congruent pairs (0.0112). Accordingly, the scatter plots in Figure 7 visually

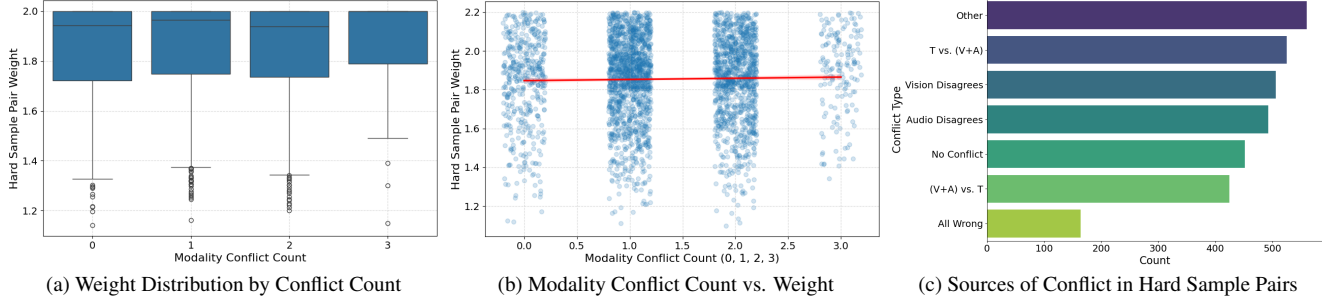


Figure 6. Analysis of the nature of difficulty in CMU-MOSI (MSA). (a) and (b) show no correlation between hard sample pairs weight and modality conflict. (c) shows hard sample pairs are a diverse mix, including 14.5% with “No Conflict”.

Table 7. Average GRPO weight by modality conflict count (T, V, A) on MUStARD. Weight correlates strongly with conflict.

Conflict Count	Average Weight	Sample Size
0	0.0085	2522
1	0.0190	1591
2	0.0500	197
3	0.4445	2

N = 4312 (total heterogeneous pairs)

Spearman’s ρ (Weight vs. Conflict Count): 0.1659

Table 8. Average GRPO weight for specific modality conflicts on the MUStARD dataset.

Conflict Type	Status	Average GRPO Weight
T-V	No Conflict	0.0112
	Conflict	0.0210
T-A	No Conflict	0.0110
	Conflict	0.0356

confirm that the conflict quadrants (II and IV) host a disproportionate number of high-weight (darker, larger) sample pairs.

In an incongruent task like MSD, the GRPO advantage-weighting mechanism successfully identifies inter-modal disagreement as the dominant factor defining the “hard sample pair” to prioritize.

Summary

Contrary to being counter-intuitive, this correlation validates that our GRPO-inspired mechanism is contextually adaptive. In MSA, where consistency is key, it correctly identifies “difficulty” as distinguishing fine-grained sentiment intensities. In MSD, where irony inherently arises from incongruity, it automatically pivots to prioritize samples with high inter-modal conflict. This confirms that GRPO advantage-weighting is not just fitting noise, but is effectively targeting the semantic core of the respective multimodal tasks.

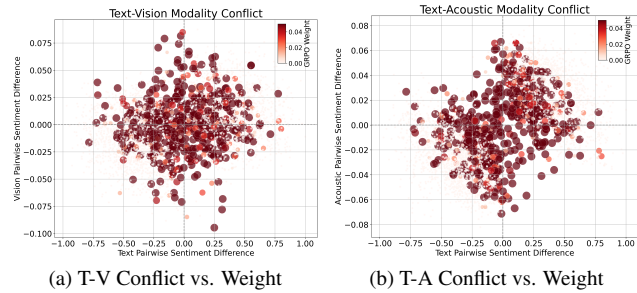


Figure 7. Analysis of the nature of difficulty in MUStARD (MSD). The scattered points of the sample pairs with specified modal conflicts fall in quadrants II and IV.



Figure 8. Model performance w.r.t the change of λ_1 and λ_2 on the CH-SIMS v2 dataset.

B.2 Hyperparameter Stability Experiments

In this section, we assess the impact of hyperparameters λ_1 and λ_2 , which denote the weights of the Group-Aware Ranking Loss and the Distribution Regularization Loss in Stage 1, respectively, on the CH-SIMS v2 [21] dataset. The results are depicted in Figure 8.

As shown in the figures, GRCF delivers consistently satisfactory performance across a broad range of settings. For λ_1 , the accuracy metrics remain remarkably stable as the value varies from 0.6 to 1.5. Notably, when λ_1 is set to 1.3, the model achieves an Acc2 of **82.6**, which surpasses the result of **81.7** reported in Table 2. Similarly, for λ_2 , performance fluctuations are marginal despite variations from 0.01 to 0.10. Interestingly, setting λ_2 to 0.04 yields a peak

Acc5 of **55.1** and Acc3 of **74.4**, again outperforming our baseline configuration.

This phenomenon demonstrates that GRCF is highly robust to the specific magnitude of loss weights. The potential of GRCF can be further unlocked through hyperparameter tuning.

B.3 Cross-Dataset Generalization

We performed a challenging zero-shot and transfer learning test to assess the robustness and generalizability of our framework’s learned representations. We trained on CMU-MOSEI and evaluated on the unseen CMU-MOSI test set.

A key technical challenge in this task is the feature dimension mismatch between the datasets (*e.g.*, MOSEI vision features have 35 dimensions, while CMU-MOSI has 47). We addressed this by implementing a feature adaptation layer in our data loader, which automatically truncates the target data to match the dimensions expected by the source-trained model.

As shown in Table 9, we observe a clear and informative divergence in the Zero-Shot model’s performance:

- **Absolute Calibration Fails:** Metrics dependent on absolute score calibration (MAE, Acc7) degrade significantly in the Zero-Shot model. The MAE (0.7388) is much worse than the In-Domain baseline. This is expected, as the Stage 2 MAE calibration overfits to the source domain’s specific score distribution.
- **Relative Ranking Generalizes:** Remarkably, metrics dependent on relative ordinal structure (Corr, Acc2, F1) are still considerable.

This finding strongly validates our GRCF framework. It demonstrates that the GRPO-inspired Stage 1 successfully learns a robust and generalizable ordinal manifold, which transfers almost perfectly to a new domain.

To further prove the generalizability of our framework, we conducted a comprehensive Transfer Learning test with two variants. The most robust approach, Transfer v2, involved taking the full CMU-MOSEI-trained model and fine-tuning it only using the Stage 2 MAE calibration task on the CMU-MOSI training set. The results are exceptional: this model, achieving an MAE of 0.594 and Acc7 of 49.6, not only fully recovers the absolute score calibration but significantly outperforms the In-Domain baseline trained from scratch on CMU-MOSI (Acc7 49.3, MAE 0.581) across all metrics. This provides strong evidence that the Stage 1 ordinal manifold learned on the larger CMU-MOSEI dataset is superior and more generalizable. The success of this Stage 2-only fine-tuning decisively proves the value of decoupling the learning of relative ranking from absolute calibration.

B.4 Modality Ablation Study during Inference

We conducted a modality ablation study to quantify the contribution of each modality. Specifically, we took our best

model (trained on all modalities of CH-SIMS v2) and evaluated it under four settings: the full modality setup (T+V+A) and three ablated setups (T+V, T+A, and T-only). During evaluation, the features of the ablated modalities were zeroed out, and their corresponding input masks were modified to simulate missing data.

The results, presented in Table 10, demonstrate the contribution of each component:

- **All modalities contribute:** The full T+V+A model (MAE 0.3053, Corr 0.6914) significantly outperforms all ablated versions, confirming that all three modalities provide useful, non-redundant information for the task.
- **Dominance of Vision:** The most informative finding is the relative impact of vision versus audio. Removing audio (T+V model) results in a moderate performance drop (MAE 0.3346). However, removing vision (T+A model) causes a much more severe degradation (MAE 0.3857, Corr 0.5446). This strongly suggests that vision is a more dominant and informative modality than audio.
- **Value of Non-verbal Cues:** The Text-Only model yields the worst performance (MAE 0.4153, Corr 0.5295), underscoring the critical importance of non-verbal signals for robust sentiment analysis.

B.5 Performance on Different Backbones

We investigate the generalizability of our framework to various linguistic encoders by substituting the default DeBERTa-v3-base text backbone with BERT-base and ALBERT-base. All models are subsequently trained and evaluated on the CMU-MOSI dataset, with performance comparisons detailed in Table 11.

GRCF maintains competitive performance even with older architectural backbones. With ALBERT, the model still achieves a strong Acc2 of 87.5, and BERT delivers a solid Acc7 of 45.6. The fact that GRCF consistently achieves high performance, regardless of the backbone, suggests that the improvements stem from our proposed Group-Aware Ranking and Calibration mechanism rather than relying solely on the strength of the text encoder.

B.6 Analysis of Model Complexity

To demonstrate that the superior performance of GRCF stems from algorithmic innovation rather than model scaling, we compare its parameter complexity against methods that utilize the DeBERTa-v3-base backbone ($\sim 184M$).

As detailed in Table 11, GRCF introduces minimal overhead, totaling 186.6M parameters. This is competitively lightweight, sitting between ITHP [44] (184.9M) and CaMIB [16] (189.2M). Given that GRCF consistently outperforms these baselines, we conclude that our gains are driven by the robust Two-Stage Ranking and Calibration design, which extracts richer semantic information without requiring a significantly larger model capacity.

Table 9. Cross-dataset generalization and transfer learning results. All models are evaluated on the CMU-MOSI test set.

Model Type	Training Data	Acc7 \uparrow	Acc2 \uparrow	F1 \uparrow	MAE \downarrow	Corr \uparrow
In-Domain	MOSI (S1+S2)	49.3	90.3	88.5	0.581	0.866
Zero-Shot	MOSEI (S1+S2)	40.0	85.8	82.9	0.739	0.816
Transfer v1	MOSEI (S1) + MOSI (S2)	49.6	88.6	86.5	0.596	0.865
Transfer v2	MOSEI (S1+S2) + MOSI (S2)	49.6	89.0	87.0	0.594	0.862

Table 10. Modality ablation results on the CH-SIMS v2 test set. The model is trained once on all three modalities (T+V+A) and evaluated by ablating (zeroing out) specific modalities.

Modalities	Acc5 \uparrow	Acc3 \uparrow	Acc2 \uparrow	F1 \uparrow	MAE \downarrow	Corr \uparrow
T + V + A	54.4	74.3	81.7	81.6	0.305	0.691
T + V	50.6	73.2	80.5	80.5	0.335	0.657
T + A	48.7	68.1	74.9	74.7	0.386	0.545
T	41.2	68.3	75.1	75.0	0.415	0.530

Table 11. Performance of GRCF with different text backbones.

Text Backbone	Acc7 \uparrow	Acc2 \uparrow	F1 \uparrow	MAE \downarrow	Corr \uparrow
DeBERTa-Base	49.3	90.3	88.5	0.581	0.866
ALBERT-Base	43.8	87.5	85.1	0.708	0.797
BERT-Base	45.6	84.1	81.2	0.736	0.793

Table 12. Parameter breakdown of GRCF and complexity comparison with other regression models.

Model / Component	Number of Parameters
<i>GRCF Detailed Breakdown</i>	
Text Encoder	183,831,552
Vision Pooler	48
Audio Pooler	75
Vision Norm	1,536
Audio Norm	1,536
Vision Projection	36,864
Audio Projection	57,600
Fusion Layer	1,770,240
Unified Encoder	590,592
Regression Head	295,681
GRCF (Total)	186,585,724
<i>Baseline Models (Total Parameters)</i>	
ITHP [44]	184,883,706
CaMIB [16]	189,246,280

Appendix C: Implementation Details

C.1 Datasets Introduction

We first conduct our experiment on MSA [48] datasets, then on MHD [10] and MSD [3] ones, which is a regression task that predicts a sentiment value for each video utterance, naturally aligning well with our ordinal learning. Afterwards, we extend GRCF to classification tasks (including

MHD and MSD) to verify the generalizability of MOAC.

- **CMU-MOSI** [48]: The CMU-MOSI dataset, released by Carnegie Mellon University’s MultiComp Lab in 2016, contains 93 YouTube videos with 2,199 opinion segments from 89 speakers. Each segment is annotated with trimodal (linguistic, visual, acoustic) sentiment intensity labels from -3 to +3 by five annotators. As the first opinion-level multimodal sentiment dataset, it serves as a standard benchmark for MSA research.
- **CMU-MOSEI** [51]: CMU-MOSEI (Multimodal Opinion Sentiment and Emotion Intensity) is a large-scale benchmark dataset for MSA, extending the earlier CMU-MOSI dataset. While CMU-MOSI contains around 2,000 annotated video utterances from a limited number of speakers, CMU-MOSEI significantly scales up in size and diversity—comprising over 22,000 utterances from more than 1,000 speakers across 250 distinct topics. Both datasets offer sentiment annotations on a Likert scale from -3 (strongly negative) to 3 (strongly positive), but CMU-MOSEI additionally includes categorical emotion labels across six classes. This makes CMU-MOSEI more suitable for training deep models with greater generalizability across sentiment and emotion recognition tasks.
- **CH-SIMS v2** [21]: CH-SIMS v2 is an improved MSA dataset based on the original CH-SIMS. It features enhanced synchronization and consistency across text, audio, and visual modalities. By addressing alignment and annotation issues, CH-SIMS v2 provides a more reliable benchmark for studying and evaluating multimodal sentiment understanding models.
- **MUSTARD** [3]: MUSTARD (Multimodal Sarcasm Detection Dataset) is a benchmark dataset for the task of multimodal sarcasm detection. It comprises 690 video utterances sourced from popular TV shows such as Friends, The Big Bang Theory, and The Golden Girls. Each instance includes a punchline along with its preceding conversational context, aligned across textual, acoustic, and visual modalities. Utterances are manually annotated as either sarcastic or non-sarcastic, enabling models to learn sarcasm not only from language but also from prosodic and visual cues.
- **UR-FUNNY v2** [10]: UR-FUNNY v2 is an extended version of the UR-FUNNY dataset designed for the Multimodal Humor Detection (MHD) task. It consists of video utterances collected from TED Talks, where each

instance includes a punchline (i.e., the humorous utterance) along with preceding context utterances from the same speaker. These are aligned across textual, acoustic, and visual modalities. Punchlines are identified based on audience laughter cues in the transcripts, while negative (non-humorous) samples lack such cues. The dataset provides improved annotations and expanded size over the original version, enabling more robust training and evaluation of models for multimodal humor understanding.

C.2 Data Format and Sampling Strategy

To effectively train our pairwise ranking model while maintaining compatibility with standard evaluation protocols, we adopt different data loading formats for different sets.

Training Set: For each training set with N original samples $\{(x_i, y_i)\}_{i=1}^N$, we generate M pairs through random sampling, where M is determined based on the dataset size. Each sample pair consists of two randomly selected utterances (x_i, y_i) and (x_j, y_j) , with a comparison label:

$$c_{ij} = \begin{cases} 1 & \text{if } y_i > y_j \\ 0 & \text{if } y_i \leq y_j \end{cases} \quad (27)$$

The training data is thus represented as (x_i, x_j, c_{ij}) , which significantly expands the training set (e.g., CMU-MOSI: 1,281 samples \rightarrow 50,000 pairs). Crucially, we maintain this pairwise format throughout all training stages (Stage 1 and Stage 2). This ensures distributional consistency between stages, preserves the ranking capabilities learned in Stage 1, and provides implicit contrastive regularization during Stage 2 calibration.

Validation and Test Sets: We maintain the original point-wise format $\{(x_i, y_i)\}_{i=1}^N$ for test data loading, where the model processes individual utterances. However, evaluation on validation sets is conducted in two complementary ways: The validation data is formatted into pairs to compute the PairwiseAcc metric. The validation data is kept in its original point-wise format to compute regression metrics (MAE, Corr) and classification metrics (Acc 2/7, F1). This is done by comparing the predicted scores \hat{y}_i against the ground-truth labels y_i for each sample. This dual evaluation strategy allows us to assess both the model’s absolute prediction accuracy and its ranking capability while maintaining fair comparison with existing methods.

C.3 Hyperparameter Optimization

We employ the Optuna [1] to conduct an automated hyperparameter search. To ensure the stability of our two-stage training pipeline, we decouple the optimization process:

- **Stage 1 Optimization:** The objective is to maximize the PairwiseAcc on the validation set. This stage prioritizes establishing a correct ordinal structure.
- **Stage 2 Optimization:** The objective shifts to minimizing the MAE to calibrate the absolute prediction values.

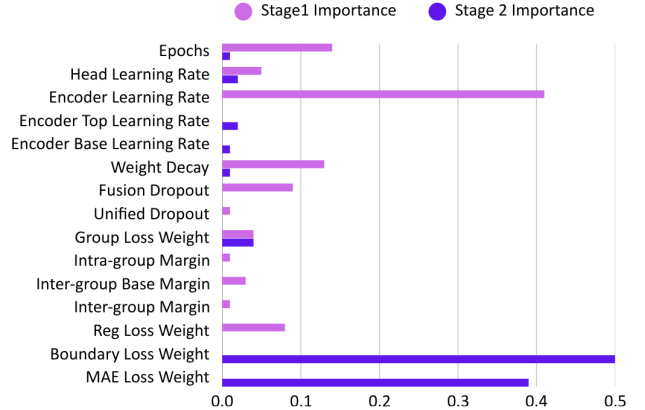


Figure 9. Hyperparameter Importance on the CMU-MOSI dataset.

The specific optimal values for each dataset are detailed in Table 13. Furthermore, to understand the sensitivity of our framework, we conduct a hyperparameter importance analysis using evaluator based on the Random Forest algorithm, as visualized in Figure 9. The results highlight that the Encoder Learning Rate is the most critical factor in Stage 1, emphasizing the need to carefully balance the retention of pre-trained knowledge with the learning of new ordinal constraints. In Stage 2, the Boundary Loss Weight emerges as significant, confirming its role in preventing score drift during calibration.

To better understand the performance of GRCF, we visualized its true and predicted values, with results presented in Figure 10.

C.4 Baselines Introduction

- **MFM [36]:** MFM factorizes multimodal features into modality-invariant discriminative and modality-specific generative factors to enhance representation learning and interpretability in multimodal tasks.
- **Self-MM [47]:** Self-MM learns modality-specific representations via self-supervised multi-task learning by generating pseudo unimodal labels without manual annotation, boosting performance in MSA.
- **AtCAF [15]:** AtCAF introduces a causality-aware attention mechanism to effectively fuse multimodal information by capturing modality-wise causal dependencies for robust MSA.
- **DLF [40]:** DLF introduces a dual-level fusion strategy that leverages both intra- and inter-modal interactions through hierarchical fusion modules to enhance MSA.
- **KuDA [7]:** KuDA employs a knowledge-enhanced dynamic attention mechanism to adaptively weigh cross-modal information, improving sentiment prediction in multimodal tasks.
- **DEVA [43]:** DEVA enhances multimodal sentiment modeling by generating textual emotional descriptions for au-

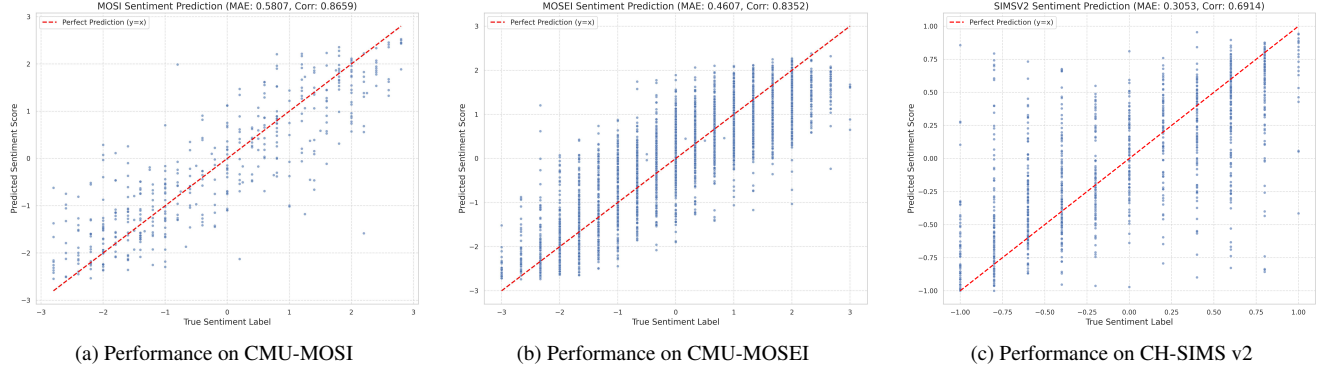


Figure 10. Ground Truth vs. Predictions Across Datasets.

Table 13. Comparison of key hyperparameters for the GRCF framework across different datasets. LR refers to learning rate. Optimal values are rounded to one significant figure for clarity.

Parameter	MOSI	MOSEI	SIMS v2
<i>General Settings</i>			
Optimizer	AdamW	AdamW	AdamW
Batch Size (per device)	96	96	96
Gradient Accumulation	8	8	8
Effective Batch Size	768	768	768
Seed	42	42	42
Score Bins Config	overlap,5	overlap,5	overlap,5
Inter-Group Margin Step	0.1	0.1	0.1
<i>Stage 1</i>			
Epochs	17	30	16
Head LR	1×10^{-5}	1×10^{-5}	3×10^{-5}
Encoder LR	8×10^{-6}	1×10^{-5}	4×10^{-6}
Weight Decay	2×10^{-2}	2×10^{-4}	1×10^{-4}
Fusion Dropout	4×10^{-1}	2×10^{-1}	3×10^{-1}
Unified Dropout	2×10^{-1}	5×10^{-1}	5×10^{-1}
Group Loss Weight	9×10^{-1}	1	1
Intra-group Margin	1×10^{-1}	9×10^{-2}	3×10^{-2}
Inter-group Base Margin	5×10^{-1}	2×10^{-1}	1×10^{-1}
Reg Loss Weight	5×10^{-3}	3×10^{-2}	6×10^{-2}
Reg Loss Margin	1	1	3×10^{-1}
Boundary Loss Weight	1×10^{-3}	5×10^{-4}	2×10^{-1}
<i>Stage 2</i>			
Epochs	5	9	18
Weight Decay	1×10^{-2}	4×10^{-3}	5×10^{-3}
Head LR	1×10^{-4}	4×10^{-5}	1×10^{-4}
Encoder Top LR	4×10^{-5}	2×10^{-5}	6×10^{-5}
Encoder Base LR	2×10^{-5}	2×10^{-6}	2×10^{-6}
Group Loss Weight	3×10^{-1}	8×10^{-1}	1
MAE Loss Weight	3×10^{-1}	2	3
Boundary Loss Weight	2×10^{-2}	7×10^{-3}	1

dio and visual cues and progressively fusing them under text guidance to strengthen fine-grained emotional representation.

sentation.

- **C-MIB [23]:** C-MIB introduces a contrastive mutual information bottleneck framework that maximizes task-relevant multimodal information while filtering out redundant signals through a global-local contrastive loss and modality dropout training.
- **ITHP [44]:** This neuroscience-inspired approach ranks modalities by information richness and processes them hierarchically through successive information bottleneck layers, where secondary modalities act as filters to distill and retain only relevant information from the primary modality, creating compact multimodal representations.
- **Multimodal Boosting [24]:** Multimodal Boosting proposes a novel boosting-based ensemble learning framework that adaptively combines weak multimodal experts to improve classification performance across modalities.
- **CaMIB [16]:** CaMIB proposes a causal multimodal information bottleneck framework that filters unimodal noise, disentangles causal and shortcut substructures via a learnable mask generator, and employs instrumental variables together with backdoor intervention to improve robustness under distribution shifts.
- **DMD [18]:** DMD introduces a modality decorrelation mechanism that explicitly separates modality-specific and shared information to improve the robustness and generalization of multimodal representations.
- **EMOE [6]:** EMOE proposes an Explainable Multimodal Emotion recognition framework that integrates regression with modality-specific attention to enhance both prediction performance and interpretability.
- **TMSON [45]:** TMSON estimates uncertainty distributions for each modality, fuses them using Bayesian rules to obtain robust multimodal representations, and employs ordinal regression with triplet loss to establish a sentiment space aware of ordinal relationships between emotion categories.
- **MOAC [25]:** MOAC introduces label-level ordinal learning that encourages samples with larger annotated labels

to receive higher predicted values through comparison-based optimization, and feature-level ordinal learning that computes feature differences between sample pairs to generate enriched features, while incorporating a neutral embedding to facilitate ordinal learning during prediction and reduce prediction difficulty.

- **EF-LSTM** [42]: An input-level multimodal fusion approach that concatenates aligned audio, video, and text features before processing them through Bidirectional LSTM layers, enabling the model to jointly learn temporal patterns and cross-modal interactions for multi-label emotion classification and intensity regression.
- **LF-DNN** [41]: A decision-level fusion approach that trains separate DNN classifiers for each modality (CNN for audio/video, BLSTM for text) and combines their predictions through a weighted ensemble layer, learning optimal modality weights during final training without intermediate feature concatenation.
- **TFN** [49]: TFN uses a three-fold Cartesian product to explicitly model unimodal, bimodal, and trimodal interactions through tensor fusion, enabling end-to-end learning of intra-modality and inter-modality dynamics for MSA.
- **LMF** [22]: LMF leverages modality-specific low-rank tensor decomposition to efficiently fuse multimodal representations, scaling linearly with the number of modalities while maintaining competitive performance.
- **MFN** [50]: MFN employs a System of LSTMs to model view-specific interactions, a Delta-memory Attention Network (DMAN) to discover cross-view interactions by attending to memory changes across timesteps, and a Multi-view Gated Memory to store cross-view interactions over time for multi-view sequential learning.
- **Graph-MFN** [51]: Graph-MFN replaces MFN’s fusion component with a Dynamic Fusion Graph (DFG) that uses interpretable efficacies to dynamically control hierarchical n-modal interactions across unimodal, bimodal, and trimodal vertices for multimodal language understanding.
- **MISA** [11]: MISA projects each modality into two distinct subspaces—modality-invariant for learning commonalities with distributional alignment and modality-specific for capturing characteristic features—to provide comprehensive representations for multimodal fusion.
- **MAG-BERT** [30]: MAG-BERT introduces a multimodal adaptation gate that shifts BERT’s internal lexical representations by incorporating visual and acoustic information, enabling the pre-trained transformer to effectively process multimodal data during fine-tuning.
- **MMIM** [9]: MMIM hierarchically maximizes mutual information between unimodal input pairs and between fusion results and unimodal representations to preserve task-related information throughout the multimodal fusion process.

- **AV-MC** [21]: AV-MC applies mixup augmentation to acoustic and visual modalities and enforces prediction consistency between original and mixed representations to enhance non-verbal cue learning in MSA.

C.5 Evaluation Metrics

The evaluation metrics employed in our experiments vary according to the characteristics and annotation schemes of different datasets:

For CMU-MOSI and CMU-MOSEI: We adopt six key metrics: (1) PairwiseAcc measures the pairwise ranking accuracy by computing the proportion of correctly ordered sample pairs, which directly evaluates the model’s ability to preserve ordinal relationships:

$$\text{PairwiseAcc} = \frac{1}{\binom{N}{2}} \sum_{i < j} \mathbb{I}[(y_i > y_j) \Leftrightarrow (\hat{y}_i > \hat{y}_j)] \quad (28)$$

where N is the number of samples, y_i and \hat{y}_i denote the ground-truth and predicted sentiment scores respectively, and $\mathbb{I}[\cdot]$ is the indicator function; (2) Acc7 measures the seven-class classification accuracy by rounding predictions to the nearest integer within $[-3, 3]$; (3) Acc2 evaluates binary classification performance distinguishing positive from negative sentiments, with samples whose ground-truth scores equal zero excluded; (4) F1 computes the harmonic mean of precision and recall for binary sentiment classification, excluding samples with ground-truth scores of zero; (5) MAE calculates the mean absolute error quantifying the deviation between predicted and ground-truth sentiment values; (6) Corr represents the correlation coefficient measuring the linear relationship between model predictions and human annotations.

For CH-SIMS v2: The following metrics are utilized: (1) PairwiseAcc follows the same definition as described above for CMU-MOSI and CMU-MOSEI; (2) Acc5 evaluates five-way sentiment classification by mapping continuous scores into five ordinal categories following the official CH-SIMS annotation protocol; (3) Acc3 evaluates three-class categorization (positive, neutral, negative); (4) Acc2, F1, MAE, and Corr follow the same definitions as described for CMU-MOSI and CMU-MOSEI.

For MUStARD and UR-FUNNY v2: Acc2 is utilized to assess the accuracy of binary classification.